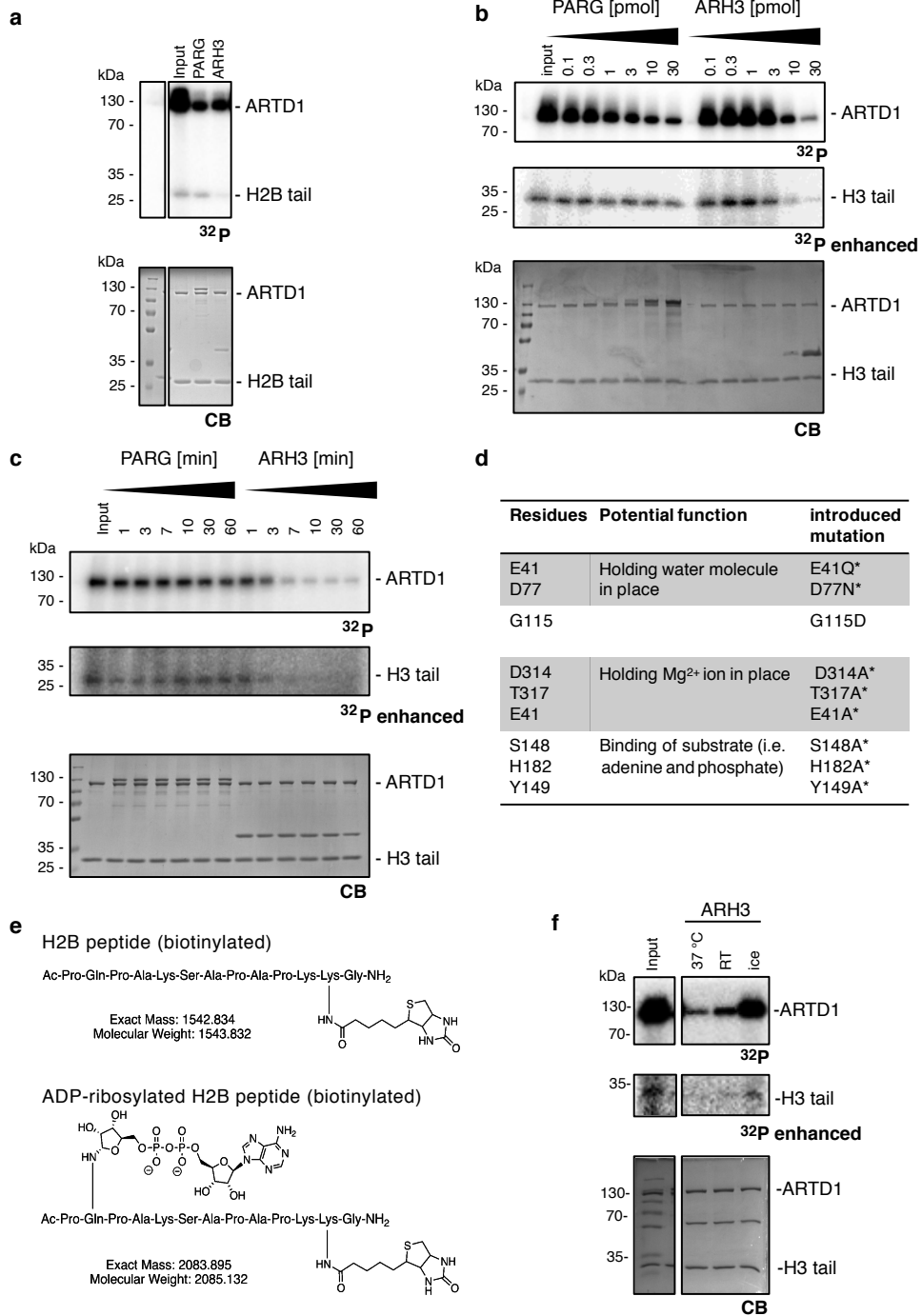


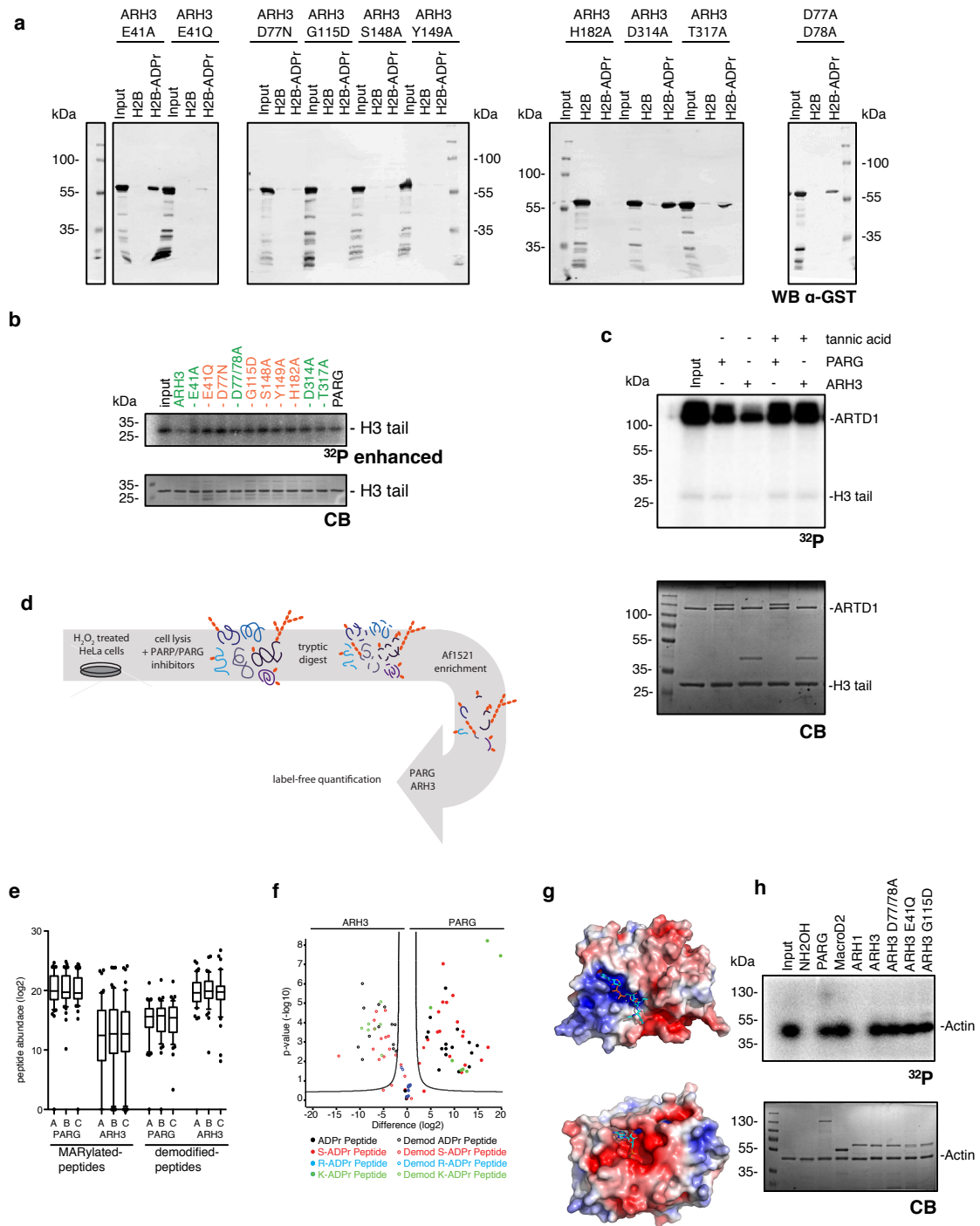
Supplementary Information

Supplementary Figure 1



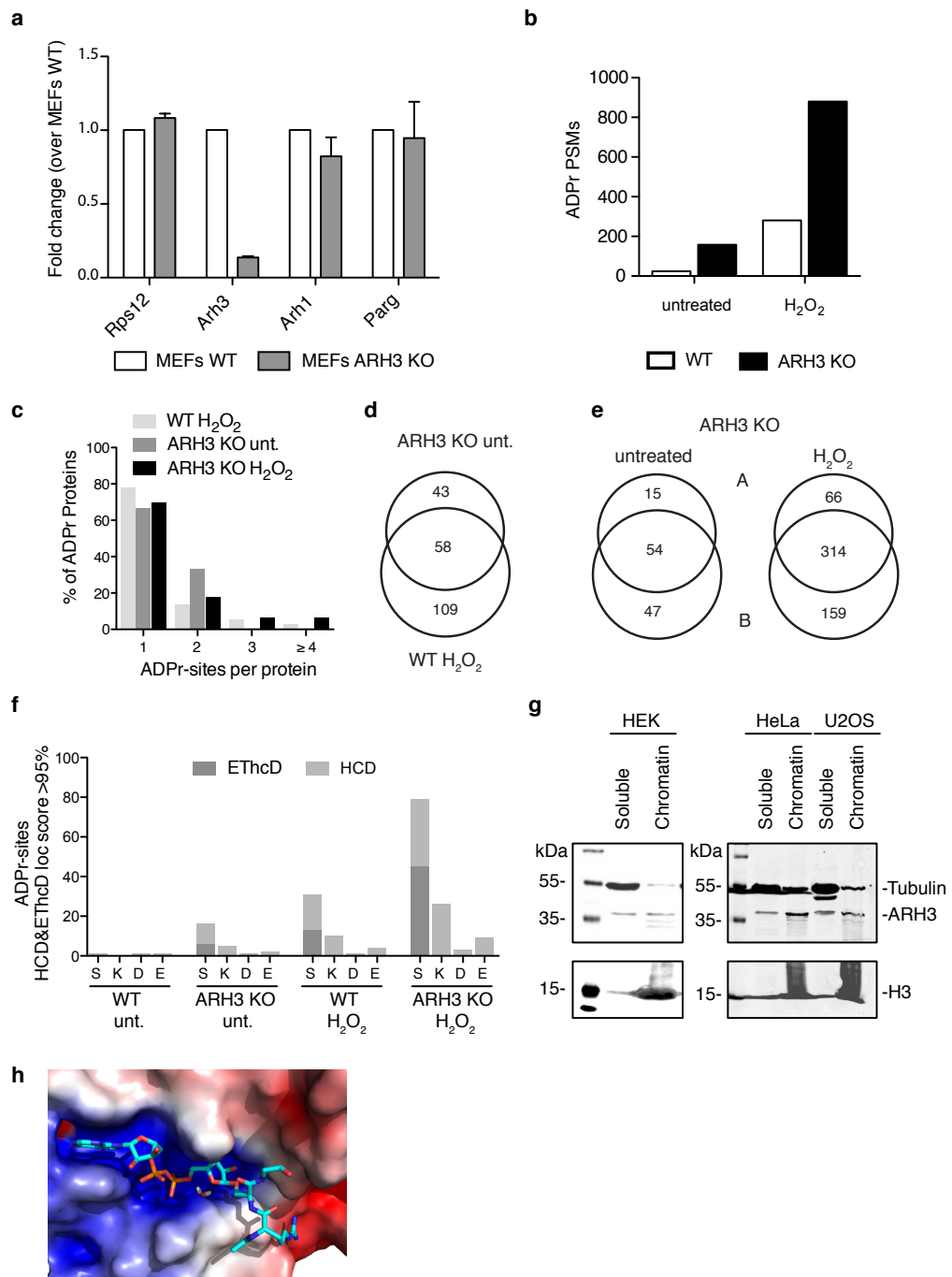
Supplementary Figure 1: (a) Recombinant H2B histone tail was *in vitro* ADP-ribosylated using recombinant ARTD1 in the presence of ^{32}P -labeled NAD^+ . Equal fractions were left untreated (Input) or were treated with PARG or ARH3. Above: radioactivity exposure, below: Coomassie Blue-stained poly-acrylamide gel. (b) Dose response of ARH3 and PARG on auto-modified ARTD1 and transmodified H3 histone tail (numbers indicate pmol of PARG and ARH3 used for demodification). (c) Time course of PARG and ARH3 activity on auto-modified ARTD1 and transmodified H3 histone tail (numbers indicate duration of the PARG and ARH3 demodification reaction in min). (d) Scheme representing the cloned and purified ARH3 mutants that were used for binding and demodification assays. (e) Schematic structure of the biotinylated H2B peptides with and without ADPr-modification. (f) Recombinant H3 histone tail was *in vitro* ADP-ribosylated using recombinant ARTD1 in the presence of ^{32}P -labeled NAD^+ . Equal fractions were left untreated (Input) or were treated with ARH3 at different temperatures. Above: radioactivity exposure, below: Coomassie Blue-stained poly-acrylamide gel.

Supplementary Figure 2



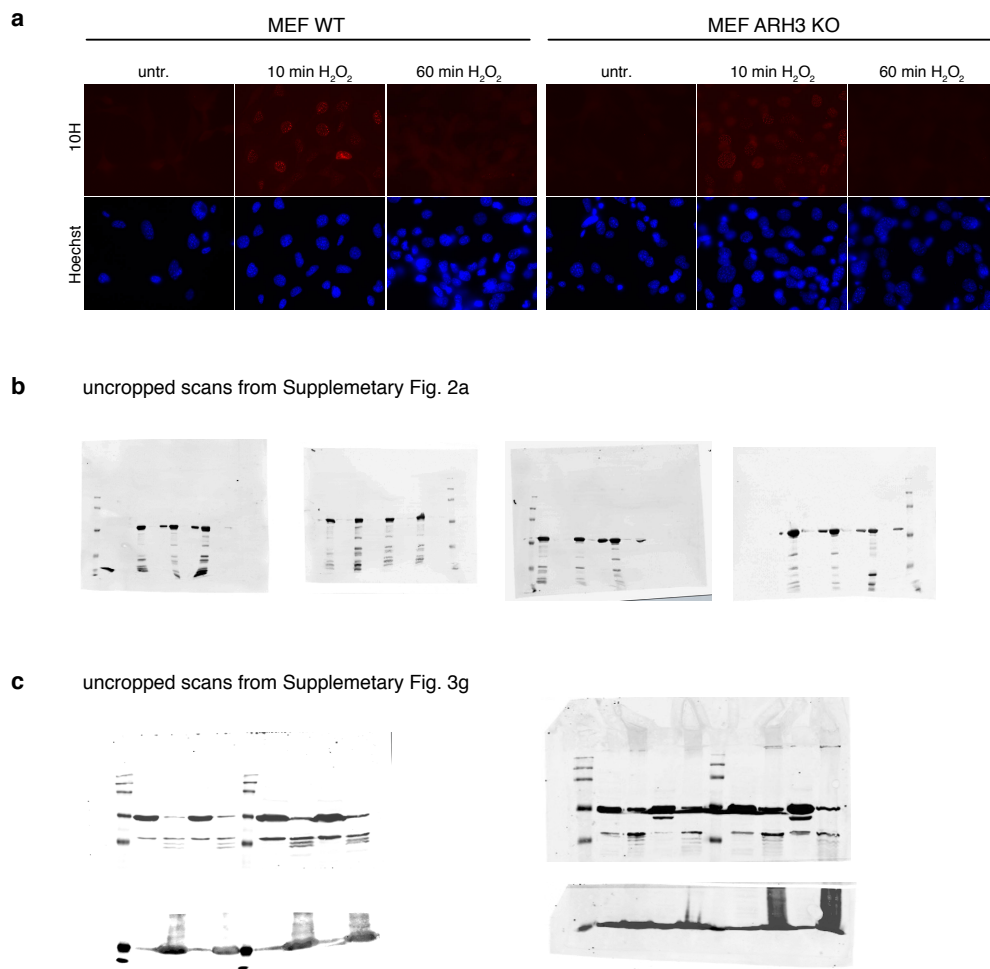
Supplementary Figure 2: (a) Western blot of pull-downs of GST-ARH3 mutants using the biotinylated peptides with (H2B-ADPr) and without (H2B) modification for assessment of binding capacity of ARH3 mutants to MARylated peptides. The blots were probed with an anti-GST antibody. (b) Recombinant H3 histone tail was *in vitro* ADP-ribosylated using recombinant ARTD1 in the presence of ^{32}P -labeled NAD^+ . Equal fractions were left untreated (Input) or were treated with PARG, wildtype and mutant ARH3. Above: radioactivity exposure, below: Coomassie Blue-stained poly-acrylamide gel. (c) Recombinant H3 histone tail was *in vitro* ADP-ribosylated using recombinant ARTD1 in the presence of ^{32}P -labeled NAD^+ . Equal fractions were left untreated (Input) or were treated with PARG and ARH3 without or in presence of tannic acid. Above: radioactivity exposure, below: Coomassie Blue-stained poly-acrylamide gel. (d) Schematic representation of the sample preparation for the LFQ MS experiment. For details see Materials and Methods. (e) Normalized abundance of individual ADP-ribosylated or demodified peptide species from three peptide preparations (A, B, C) that were treated with either ARH3 or PARG. (f) Volcano plot as in Figure 2c using high scoring EThcD and HCD fragmentation spectra. ‘Demodified peptides’ are shown as open circles and ‘ADP-ribosylated peptides’ as filled circles. Confident ADP-ribosylation sites identified by EThcD and HCD are annotated and color coded in red as S-ADPr, in blue as R-ADPr sites and in green as K-ADPr sites. ADP-ribosylated peptides with uncertain ADP-ribosylation site localization are shown in black. The black hyperbolic line represents a permutation-based False Discovery Rate (FDR) of 5% and a minimal fold change of 2. (g) Comparison of ARH3 (PDB code: 2FP0, with a modeled ADP-ribosylated serine within an acetyl lysine-serine-glycine (KSG) tripeptide in the binding site) and ARH1 (PDB code: 3HFW, with adenosine diphosphate). Protein surfaces are colored according to electrostatic potential (on a scale of -5 to 5 kT/e). (h) Actin was *in vitro* ADP-ribosylated with the bacterial toxin CD $\text{T}\alpha$ in the presence of ^{32}P -labeled NAD^+ . Equal fractions were left untreated (Input) or were treated with hydroxylamine, PARG, MACROD2, ARH1, wildtype and mutant ARH3. Above: radioactivity exposure, below: Coomassie Blue-stained poly-acrylamide gel.

Supplementary Figure 3



Supplementary Figure 3: (a) mRNA levels of *Rps12* (house keeping gene), *Arh3*, *Arh1* and *Parg* in untreated ARH3 WT and KO MEF cells assessed by qRT-PCR. Data represent means \pm SEM for $n = 3$ independent experiments. (b) ADP-ribosylated peptide spectra matches of WT and ARH3 KO cells in untreated and hydrogen peroxide-treated conditions. (c) Number of ADPr sites per protein. (d) Venn diagrams of unique ADP-ribosylated peptides from H₂O₂-treated WT and untreated ARH3 KO MEFs as in Fig. 3a. (e) Venn diagrams of unique ADP-ribosylated peptides identified in biological replicates (samples A and B). (f) Number of unique ADP-ribose acceptor amino acids localized with EThcD and HCD. (g) Chromatin extraction of HEK, HeLa and U2OS cells followed by western blot analysis with α -tubulin (predominantly found in the soluble fraction), α -H3 (marking the chromatin-bound fraction) and α -ARH3 (detected in both fractions). (h) Energy minimized binding mode of an acetyl-RSG peptide with ADPr-Ser modified. The surface of ARH3 (including the binding site magnesium ions) is colored according to electrostatic potential. The positively charged amino group of the R side chain and backbone amide groups point towards the region of the surface with negative potential.

Supplementary Figure 4



Supplementary Figure 4: (a) Immunofluorescence pictures showing PAR-staining in WT and ARH3 KO MEF cells. **(b)** Full blots for Supplementary Fig. 2a. **(c)** Full blots for Supplementary Fig. 3g.